High ellipticity of harmonics from molecules in strong laser fields of small ellipticity

F. J. Sun,[1] C. Chen,[1,2,*] W. Y. Li,[3] X. Liu,[4] W. Li,[4] and Y. J. Chen[1,†]

[1]*College of Physics and Information Technology, Shaanxi Normal University, Xi'an 710119, China*

[2]*School of Physics, Hebei Normal University, Shijiazhuang 050024, China*

[3]*School of Mathematics and Science, Hebei GEO University, Shijiazhuang 050031, China*

[4]*Beijing Institute of Space Mechanics and Electricity, Chinese Academy of Space Technology, Beijing 100094, China*

(Received 15 January 2021; revised 20 April 2021; accepted 21 April 2021; published 10 May 2021)

We study high-order harmonic generation (HHG) from aligned molecules in strong elliptically polarized laser fields numerically and analytically. Our simulations show that the spectra and polarization of HHG depend strongly on the molecular alignment and the laser ellipticity. In particular, for small laser ellipticity, large ellipticity of harmonics with high intensity is observed for parallel alignment, along with forming a striking ellipticity hump around the threshold. We show that the interplay of the molecular structure and two-dimensional electron motion plays an important role here. This phenomenon can be used to generate bright elliptically polarized extreme ultraviolet pulses.

DOI: 10.1103/PhysRevA.103.053108

I. INTRODUCTION

In recent decades, high-order harmonic generation (HHG) from atoms [1–3], molecules [4–6], and solids [7–9] has been a hot subject in experimental and theoretical studies of strong laser-matter interaction. HHG has shown promising applications as a seed to generate attosecond pulses. It can also be used as a unique tool to probe the ultrafast dynamics of electrons within atoms and molecules with unprecedent attosecond resolution.

HHG can be well understood with the classical [10] and quantum [11] three-step models. These models describe HHG as a three-step process: (i) the valence electron of atoms or molecules is ionized by the laser field, (ii) the freed electron propagates in the external field, and (iii) the electron is driven by the laser field to return to and recombine with the parent ions with the emission of a high-energy harmonic along the direction parallel to the laser polarization (parallel harmonic). The quantum model [11], frequently termed the strong-field approximation (SFA), also predicts the emission of harmonics along the direction perpendicular to the laser polarization (perpendicular harmonic). For a linear symmetric molecule exposed to a strong linearly polarized laser field, due to the symmetry of the laser-driven system, the perpendicular harmonics appear only for molecular targets aligned along a direction not parallel or perpendicular to the laser polarization [12]. According to the SFA, parallel and perpendicular harmonics are emitted at the same instant and have no phase differences between them. So the whole harmonics emitted are also linearly polarized.

Experimental studies indeed have observed the elliptical polarization of harmonics emitted from aligned molecules in the linearly polarized laser field [12]. This polarization effect of HHG has attracted a great deal of attention in recent years, as it implies that one can acquire elliptically polarized extreme ultraviolet (EUV) ultrashort pulses with HHG in a linearly polarized laser field [13]. A great many experimental and theoretical efforts have been devoted to the complex origins of this HHG polarization [14–20]. On the whole, this polarization is associated with the atomic or molecular properties in strong laser fields. It occurs for the harmonics whose parallel or perpendicular components are subject to certain destructive interferences so that different contributions are involved in the emission of these two components, resulting in an inherent phase difference between them.

When a two-dimensional (2D) laser field is used, such as an elliptically polarized laser field [21–27], it is natural to think that the HHG from both atoms and molecules in such laser fields is also elliptically polarized. However, in this case, how the molecular properties will affect this polarization is not very clear, especially when the minor component of the 2D laser field is weak so that it destroys the symmetry of the laser-driven system but does not have a remarkable influence on the electron dynamics.

In this paper, we focus on the polarization of HHG from aligned molecules [28,29] in strong elliptical laser fields with small ellipticity. When the spectral properties of such HHG have been studied widely [30–34], the polarization properties of the relevant HHG are less explored. We focus on whether it is possible to obtain a bright and ultrashort pulse with large ellipticity using HHG polarization of molecules in such laser fields.

Based on the numerical solution of the time-dependent Schrödinger equation (TDSE) and the SFA, our simulations show that the polarization of HHG from H_2^+ is strongly dependent on the molecular alignment and the laser ellipticity. The HHG of the molecule shows striking elliptical polarization located at some harmonic energy, and this location

*chenchao1202@163.com

†chenyjhb@gmail.com

shifts toward higher energy as the alignment angle θ (the angle between the molecular axis and the main component of the elliptical laser field) is increased. In particular, for parallel alignment of the molecule, for which the HHG elliptical polarization does not occur in a linearly polarized laser field, the harmonics around the threshold show large ellipticity for a small laser ellipticity, along with forming a striking ellipticity hump located at a wide energy region. This phenomenon can be attributed to the interplay of the molecular structure and laser-induced 2D electron dynamics. The small component of the elliptical laser field destroys the symmetry of the laser-driven system at $\theta = 0^\circ$, allowing the emission of strong perpendicular harmonics near the threshold at this angle. The quantum-mechanical uncertainty of the electron wave-packet motion has different effects on the phases of parallel and perpendicular near-threshold harmonics, resulting in large ellipticity of the harmonics. At the same time, the effects associated with the multiple-center characteristic of the molecular structure increase the range of harmonics with large ellipticity, along with forming the ellipticity hump. This phenomenon holds as we change the internuclear distance and the molecular species. Because near-threshold harmonics including both parallel and perpendicular components generally have remarkably higher intensities than those in the HHG plateau, the ellipticity hump for parallel alignment can be used to obtain a strong elliptically polarized EUV pulse.

II. THEORETICAL METHODS

A. Numerical method

We assume that the main component of the elliptical laser field is polarized along the direction parallel to the x axis, and the minor component is along the y axis. In addition, the molecular axis is located in the xy plane. Then the elliptical electric field can be written as $\mathbf{E}(t) = \mathbf{e}_x E_x(t) + \mathbf{e}_y E_y(t)$, with $E_x(t) = f(t)\mathcal{E}\sin\omega_0 t$, $E_y(t) = \varepsilon f(t)\mathcal{E}\sin(\omega_0 t + \phi)$, and $\phi = \pi/2$. $\mathbf{e}_x$ ($\mathbf{e}_y$) is the unit vector along the x (y) axis [i.e., the major (minor) axis of the polarization ellipse]. ε is the laser ellipticity, ω_0 is the laser frequency, and $f(t)$ is the envelope function. $\mathcal{E} \equiv \mathcal{E}(\varepsilon) = \mathcal{E}_0/\sqrt{(1+\varepsilon^2)}$, and $\mathcal{E}_0$ is the laser amplitude relating to the peak laser intensity I.

In the length gauge, the Hamiltonian of the molecule interacting with the elliptical laser field can be written as $H(t) = \mathbf{p}^2/2 + V(\mathbf{r}) + \mathbf{r}\cdot\mathbf{E}(t)$ (in atomic units of $\hbar = e = m_e = 1$). Here, $V(\mathbf{r})$ is the Coulomb potential of the molecule. For the H_2^+ system first explored in the paper, the potential $V(\mathbf{r})$ used has the form $V(\mathbf{r}) = -Z/\sqrt{\zeta + \mathbf{r}_1^2} - Z/\sqrt{\zeta + \mathbf{r}_2^2}$, with $\mathbf{r}_{1(2)}^2 = (x \pm \frac{R}{2}\cos\theta)^2 + (y \pm \frac{R}{2}\sin\theta)^2$ in 2D cases. Here, $\zeta = 0.5$ is the smoothing parameter, which is used to avoid the Coulomb singularity, and θ is the alignment angle. Z is the effective nuclear charge, which is adjusted such that the ionization energy of the model molecule at the internuclear distance R is $I_p = 1.1$ a.u. Typically, for the equilibrium separation of $R = 2$ a.u., we have $Z = 1$.

Numerically, the TDSE of $i\dot{\Psi}(t) = H(t)\Psi(t)$ is solved with the spectral method [35]. We use a grid size of $L_x \times L_y = 204.8 \times 204.8$ a.u. with a grid spacing of $\Delta x = \Delta y = 0.2$ a.u. for the x and y axis, respectively. To eliminate the spurious reflections of the wave packet from the boundary, a mask function $F(r)$ is used in the boundary to absorb the continuum wave packet. For the x direction, we have used $F(x) = \cos^{1/8}[\pi(|x| - x_0)/(L_x - 2x_0)]$ for $|x| \geqslant x_0$ and $F(x) = 1$ for $|x| < x_0$. Here $x_0 = L_x/8$ is the boundary of the absorbing procedure. The situation is similar for the y direction. Alternatively, we can set the boundary of the absorbing procedure along the x direction (i.e., the direction of the main polarization component of the elliptical laser field) as $x_0 = 0.9x_m$ with $y_0 = L_y/8$ in the y direction unchanged [18]. Here, $x_m = \mathcal{E}/\omega_0^2$ is the maximal displacement of the electron as it travels in the laser field following the short trajectory. In linearly polarized cases, it has been shown that this treatment removes the contributions of the long trajectory and multiple returns to HHG, but the short-trajectory contributions are not affected. For the present elliptically polarized cases with small ellipticity, we can also use the procedure to resolve short-trajectory contributions. We will call this treatment short-trajectory simulations. The interference between long and short trajectories has an important influence on harmonic polarization [17]. As discussed in [18], to identify the angle dependence of HHG polarization in a linearly polarized laser field, short-trajectory simulations are preferred. This situation also holds in elliptical cases, as we will discuss below.

After the wave function $\Psi(t)$ is obtained, the coherent parts of the parallel and perpendicular spectra can be evaluated with Fourier transform of dipole acceleration:

$$F_{\parallel(\perp)}(\omega) = \int \langle\Psi(t)|\mathbf{e}_{x(y)}\cdot\nabla V(\mathbf{r})|\Psi(t)\rangle e^{i\omega t}dt. \qquad (1)$$

Here $\omega = n\omega_0$ is the emitted-photon frequency. Then the intensities of the harmonic components can be written as $A_{\parallel(\perp)}(\omega) = |F_{\parallel(\perp)}(\omega)|^2$.

The ellipticity of HHG, which is related to the amplitude ratio and the phase difference of the parallel and perpendicular harmonics, can be evaluated using

$$\varepsilon_h = \sqrt{\frac{1+\eta-\sqrt{1+2\eta\cos 2\delta+\eta^2}}{1+\eta+\sqrt{1+2\eta\cos 2\delta+\eta^2}}}, \qquad (2)$$

where $\delta = \phi_\parallel - \phi_\perp$ is the phase difference with $\phi_{\parallel(\perp)}(\omega) = \arg[F_{\parallel(\perp)}(\omega)]$, $\delta = k\pi + \delta_1$ with $k = 0, 1$, and $0 \leqslant \delta_1 \leqslant \pi$. The term $\eta = A_\perp(\omega)/A_\parallel(\omega)$ denotes the amplitude ratio. The subscript of the harmonic ellipticity ε_h differentiates it from the laser ellipticity ε. The range of harmonic ellipticity is $\varepsilon_h \in [0, 1]$. Equation (2) shows that high HHG ellipticity can be expected when the intensity of the perpendicular harmonic is comparable to the parallel one and there is a phase difference of $\delta_1 \sim \pi/2$ [19]. We mention that the orientation dependence of parallel and perpendicular harmonics can also be qualitatively discussed with the Floquet theorem [36].

In our simulations, we use a 10-cycle laser pulse that is linearly ramped up for two optical cycles and then kept at a constant intensity for six additional cycles and finally linearly ramped down for two optical cycles. Unless mentioned elsewhere, our discussions will be performed for a peak laser intensity of $I = 5 \times 10^{14}$ W/cm^2, a laser wavelength of $\lambda = 800$ nm, and $R = 2$ a.u.

B. Analytical description

In analytical treatments, we assume that the molecular axis is along the z axis, and the laser field $\mathbf{E}(t)$ is located in the xz plane with an angle θ between its major axis and the molecular axis. Then according to the SFA, the time-dependent dipole moment can be written as [11]

$$\mathbf{x}(t) = i\int_0^\infty d\tau\Big[\xi(\tau)\mathbf{d}_r^*[\mathbf{p}_{st}+\mathbf{A}(t)]e^{-iS(\mathbf{p}_{st},t,\tau)} \times \mathbf{E}(t-\tau)\cdot\mathbf{d}_i[\mathbf{p}_{st}+\mathbf{A}(t-\tau)]\Big] + \text{c.c.} \quad (3)$$

Here, $\tau = t - t'$ is the excursion time of the rescattering electron in the driving laser field when it is ionized at the time t', and $\xi(\tau) = (\frac{\pi}{\epsilon'+i\frac{\tau}{2}})^{\frac{3}{2}}$ with infinitesimal ϵ'. The term $\mathbf{p}_{st} \equiv \mathbf{p}_{st}(t,t') = -\frac{1}{t-t'}\int_{t'}^{t}\mathbf{A}(t'')dt''$ is the canonical momentum, and $\mathbf{A}(t) = -\int^t \mathbf{E}(t')dt'$ is the vector potential of the external field $\mathbf{E}(t)$. The term $S(\mathbf{p}_{st},t,\tau) = \int_{t'}^{t} dt''\{\frac{[\mathbf{p}_{st}+\mathbf{A}(t'')]^2}{2}+I_p\}$ is the semiclassical action. The term $\mathbf{d}_i(\mathbf{p})$ is the bound-free dipole transition matrix element between the molecular ground state $|0\rangle$ and the continuum $|\mathbf{p}\rangle$ (which is approximated with the plane wave $|e^{i\mathbf{p}\cdot\mathbf{r}}\rangle$) in the ionization step, and it can be written as $\mathbf{d}_i(\mathbf{p}) = \langle\mathbf{p}|\mathbf{r}|0\rangle = (2\pi)^{-3/2}\int d\mathbf{r}\, e^{-i\mathbf{p}\cdot\mathbf{r}}\mathbf{r}\langle\mathbf{r}|0\rangle$. Similarly, the term $\mathbf{d}_r(\mathbf{p}) = \langle\mathbf{p}_k|\mathbf{r}|0\rangle = (2\pi)^{-3/2}\int d\mathbf{r}\, e^{-i\mathbf{p}_k\cdot\mathbf{r}}\mathbf{r}\langle\mathbf{r}|0\rangle$ is that in the recombination step with the effective momentum $\mathbf{p}_k$, which considers the Coulomb correction on the momentum $\mathbf{p}$ of the continuum $|\mathbf{p}\rangle \propto |e^{i\mathbf{p}\cdot\mathbf{r}}\rangle$ in recombination. Note, this correction changes only the momentum $\mathbf{p}$ of the state $|\mathbf{p}\rangle$, assuming the energy $E_p = \mathbf{p}^2/2$ of the state $|\mathbf{p}\rangle$ is unchanged. For linearly polarized cases, one can use the expression of $\mathbf{p}_k = \frac{\mathbf{p}}{|\mathbf{p}|}p_k$ with $p_k = \sqrt{2(E_p+I_p)}$ [37]. We will discuss the form of the effective momentum $\mathbf{p}_k$ for the present elliptically polarized cases with small laser ellipticity later.

Through Fourier transform of $\mathbf{x}(t)$, the coherent part of the spectrum along the major axis $\mathbf{e}_\parallel$ of the elliptical laser field can be written as

$$F_l(\omega) = i\int dt\int_0^\infty d\tau\Big[\xi(\tau)\mathbf{e}_\parallel\cdot\mathbf{d}_r^*[\mathbf{p}_{st}+\mathbf{A}(t)] \times \mathbf{E}(t-\tau)\cdot\mathbf{d}_i[\mathbf{p}_{st}+\mathbf{A}(t-\tau)]e^{-iS(p_{st},t,\tau)}e^{i\omega t}\Big]. \quad (4)$$

The integration in the above expression can be treated with solving the saddle-point equation [11,38]

$$[\mathbf{p}_{st}+\mathbf{A}(t_s')]^2/2 + I_p = 0,$$
$$[\mathbf{p}_{st}+\mathbf{A}(t_s)]^2/2 + I_p = \omega. \quad (5)$$

The first equation describes the tunneling process with the ionization momentum $\mathbf{p}_{si} = \mathbf{p}_{st} + \mathbf{A}(t_s')$, and the second equation describes the recombination process with the recollision momentum $\mathbf{p}_{sr} = \mathbf{p}_{st} + \mathbf{A}(t_s)$. These momenta generally have complex forms in 2D laser fields. Solving the saddle-point equations, one can get the saddle-point ionization time t_s' and saddle-point return time t_s of the rescattering electron, as well as the saddle-point momentum $\mathbf{p}_{st}(t_s,t_s')$. So Eq. (4) can be simplified as

$$F_l(\omega) \propto \sum_s [G(t_s,\tau_s)\mathbf{e}_\parallel\cdot\mathbf{d}_r^*(\mathbf{p}_{sr})\mathbf{E}(t_s')\cdot\mathbf{d}_i(\mathbf{p}_{si})S_p(\omega)]. \quad (6)$$

Here, $G(t_s,\tau_s) = \xi(\tau_s)[1/\det(t_s,\tau_s)]^{1/2}$, and $\det(t_s,\tau_s)$ denotes the determinant of the 2×2 matrix formed by the second derivatives of the action with respect to t and τ [39]. The term $\tau_s = t_s - t_s'$ is the saddle-point travel time. The sum in Eq. (6) extends over all possible saddle points (t_s', t_s) for the emission of a harmonic ω. The term $S_p(\omega)$ has the form of $S_p(\omega) = e^{-i(S_s-\omega t_s)}$, with $S_s \equiv S(\mathbf{p}_{st},t_s,\tau_s)$. The real parts of the saddle points (t_s', t_s) have been considered as the ionization and return times of the electron, respectively. The saddle points have also been termed as electron trajectories, including long trajectory, short trajectory, and multiple returns. The trajectories are well resolved in the temporal region and have different ionization and return times.

In Eq. (6), these two dipoles $\mathbf{e}_s\cdot\mathbf{d}_i(\mathbf{p}_{si})$ and $\mathbf{e}_\parallel\cdot\mathbf{d}_r^*(\mathbf{p}_{sr})$ are mainly responsible for the angle dependence of HHG, as discussed in [40]. The symbol $\mathbf{e}_s$ denotes the unit vector along the laser polarization of the electric field $\mathbf{E}(t)$ at $t = t_s'$. We write the product of these two dipoles at the saddle point (t_s, t_s') as

$$M_s(\omega,\theta) = |\mathbf{e}_s\cdot\mathbf{d}_i(\mathbf{p}_{si})|^2|\mathbf{e}_\parallel\cdot\mathbf{d}_r^*(\mathbf{p}_{sr})|^2. \quad (7)$$

When describing the ground-state wave function using a linear combination of atomic orbitals–molecular orbitals (LCAO-MO) approximation, the dipole moment for H_2^+ with a $1\sigma_g$ valence orbital can be written as [37]

$$\mathbf{d}^{1\sigma_g}(\mathbf{p}) = N^{1\sigma_g}\Big[-2i\cos\Big(\frac{\mathbf{p}\cdot\mathbf{R}}{2}\Big)\mathbf{d}^{1s}(\mathbf{p})\Big]. \quad (8)$$

Here, $N^{1\sigma_g}$ is the normalization factor, and $\mathbf{R}$ is the vector between the two atomic cores of the molecule. The term $\cos(\mathbf{p}\cdot\mathbf{R}/2)$ denotes interference between these two cores, and $\mathbf{d}^{1s}(\mathbf{p})$ denotes the atomic dipole moment of a $1s$ orbital. When the laser ellipticity ε is small so that the main component of the elliptical laser field dominates the ionization, the ionization momentum p_{si} can be approximately expressed with $p_{si} \approx \pm i\kappa = \pm i\sqrt{2I_p}$ [41]. Equation (7) can then be rewritten as [37,40,42,43]

$$M_s(\omega,\theta) \propto \Big|\cos\Big(i\kappa\frac{R}{2}\cos\theta_I\Big)\Big|^2 M_s^r(\omega,\theta)M_s^a, \quad (9)$$

with

$$M_s^r(\omega,\theta) = \Big|\cos\Big(p_{sr}'\frac{R}{2}\cos\theta_R\Big)\Big|^2. \quad (10)$$

Here, $M_s^a \equiv |\,[\mathbf{e}_s\cdot\mathbf{d}_i^{1s}(\mathbf{p}_{si})][\mathbf{e}_\parallel\cdot\mathbf{d}_r^{1s*}(\mathbf{p}_{sr}')]\,|^2$, and θ_I (θ_R) is the exit (recollision) angle between the vectors $\mathbf{p}_{si}$ ($\mathbf{p}_{sr}$) and $\mathbf{R}$ [44]. In Eq. (10), we have used the effective momentum $\mathbf{p}_{sr}'$ instead of $\mathbf{p}_{sr}$ in the recombination dipole to consider the Coulomb correction, as discussed in Eq. (3). For the elliptical laser field with a small ellipticity ε explored here, the effective momentum $\mathbf{p}_{sr}'$ used has the form of $\mathbf{p}_{sr}' = \mathbf{e}_\parallel p_\parallel' + \mathbf{e}_\perp p_\perp$, with $p_{sr}' = \sqrt{p_\parallel'^2 + p_\perp^2}$. Here, the symbol $\mathbf{e}_\perp$ denotes the unit vector along the minor axis of the elliptical laser field, with $p_\parallel' = \sqrt{2[\omega-\varepsilon I_p]}$ and $p_\perp$ being the real part of the $\mathbf{e}_\perp$ component of $\mathbf{p}_{sr} = \mathbf{p}_{st} + \mathbf{A}(t_s)$ at the saddle point (t_s', t_s). Accordingly, the recollision angle θ_R has the expression of $\theta_R = \arctan(p_\perp/p_\parallel') - \theta$.

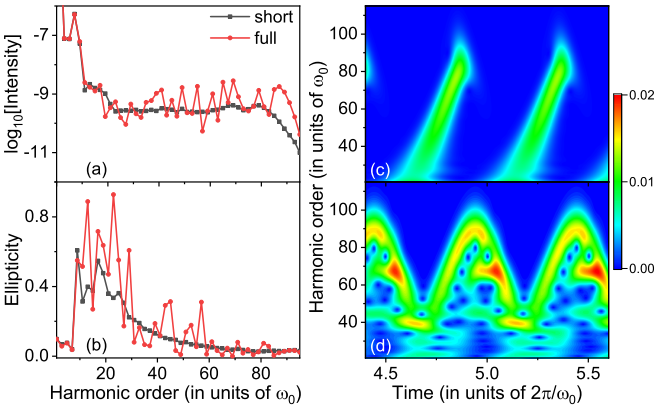

FIG. 1. Spectra (a) and ellipticity (b) of harmonics for aligned molecules H_2^+ at $\theta = 0^\circ$ and $\varepsilon = 0.1$, obtained with short-trajectory (black square) and full (red circle) TDSE simulations. In (c) and (d), we show relevant time-frequency distributions for short-trajectory (c) and full (d) simulations.

As discussed in [37], for H_2^+ in linearly polarized laser fields, the term $M_s^r(\omega, \theta)$ in Eq. (9) is the most sensitive to the molecular alignment. Our simulations show that the situation also holds for the cases of small laser ellipticity in the paper. In the following, we will compare the predictions of $M_s^r(\omega, \theta)$ of Eq. (10) with the TDSE results to understand the angle-dependent HHG ellipticity.

III. RESULTS AND DISCUSSIONS

In Fig. 1, we show the HHG results of full TDSE simulations and short-trajectory simulations at $\varepsilon = 0.1$ and $\theta = 0^\circ$. As the spectra of full simulation show the complex interference structure, the short-trajectory simulation is smoother, as seen in Fig. 1(a). Accordingly, the ellipticity of short-trajectory harmonics is also more regular than the full-simulation harmonics, with a remarkable ellipticity hump shown around the threshold, as seen in Fig. 1(b). This ellipticity hump at $\theta = 0^\circ$, which disappears in a linearly polarized laser field, is the main phenomenon we will discuss in the paper. In Fig. 1(d). the time-frequency analysis of TDSE dipole acceleration [45] also clearly shows the complex interference between different electron trajectories in full TDSE simulations, as the interference structure is basically absent in the short-trajectory results shown in Fig. 1(c). In the following, we focus on the short-trajectory results, which allow a clear identification of the angle-dependence polarization of HHG from molecules in the elliptical laser field.

To understand the polarization of HHG from aligned molecules in elliptical laser fields, in Fig. 2 we plot the TDSE short-trajectory spectra of parallel versus perpendicular harmonics of H_2^+ at different angles θ and laser ellipticity ε. For comparison, the results of a model atom with $I_p = 1.1$ a.u. are also shown.

For cases of parallel harmonics in the left column of Fig. 2, the results in each panel show that the intensities of the spectra decrease fast when the laser ellipticity is increased, reflecting the suppression of the recombination due to the lateral motion of the electron induced by the minor component of the

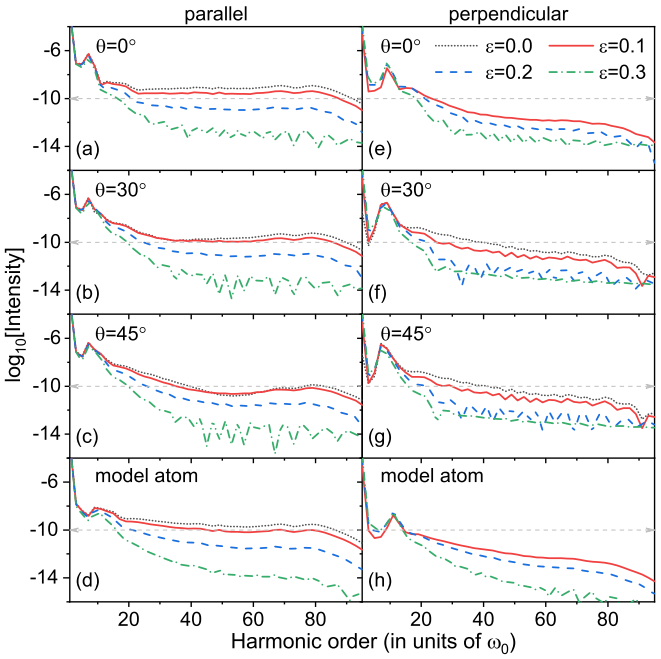

FIG. 2. Spectra of parallel (a)–(d) and perpendicular (e)–(h) harmonics for aligned molecules H_2^+ at $\theta = 0^\circ$ (a),(e), 30° (b),(f), 45° (c),(g), and for a model atom with similar I_p to H_2^+ (d),(h), with the laser ellipticity of $\varepsilon = 0$ (black dotted), $\varepsilon = 0.1$ (red solid), $\varepsilon = 0.2$ (blue dashed), and $\varepsilon = 0.3$ (green dashed-dotted). The horizontal arrows in each row are plotted to facilitate the comparison.

elliptical laser field. For cases of perpendicular harmonics, the intensities of spectra also decrease with the increase of laser ellipticity on the whole, as seen in each panel in the right column of Fig. 2. It is worth noting that for $\theta = 0^\circ$ in Fig. 2(e) and for the atom case in Fig. 2(h), the perpendicular harmonics disappear for $\varepsilon = 0$ corresponding to a linearly polarized laser field, due to the symmetry of the laser-driven system in the cases. In addition, results in Fig. 2 also show that for lower harmonic orders below the threshold (about H19), the yields of parallel and perpendicular harmonics are remarkably higher than those in the plateau regions of the spectra and are not sensitive when changing the laser ellipticity. In particular, they are comparable at small laser ellipticity, suggesting the possibility of a high harmonic ellipticity according to Eq. (2). With the help of the horizontal arrows in each panel, a careful comparison for the molecular cases also shows that both the parallel and perpendicular spectra differ for the molecular alignment, and the parallel spectra in the plateau region are stronger at $\theta = 0^\circ$ than in other cases. We will return to this point later.

In Fig. 2, our discussions are mainly concentrated on the dependence of HHG yields of parallel versus perpendicular harmonics on the laser ellipticity for a certain alignment angle. In Fig. 3, we present a comparison between HHG ellipticity and the corresponding spectra and dipoles of Eq. (10) at different angles for a certain laser ellipticity. First, for $\varepsilon = 0$ of the linearly polarized case in Fig. 3(a), the harmonics at $\theta = 30^\circ$ and 45° show large ellipticity, with an ellipticity peak formed around some harmonic energy. The position of the ellipticity peak shifts with the increase of the angle and corresponds to the minimum in the relevant parallel spectrum in Fig. 3(b).

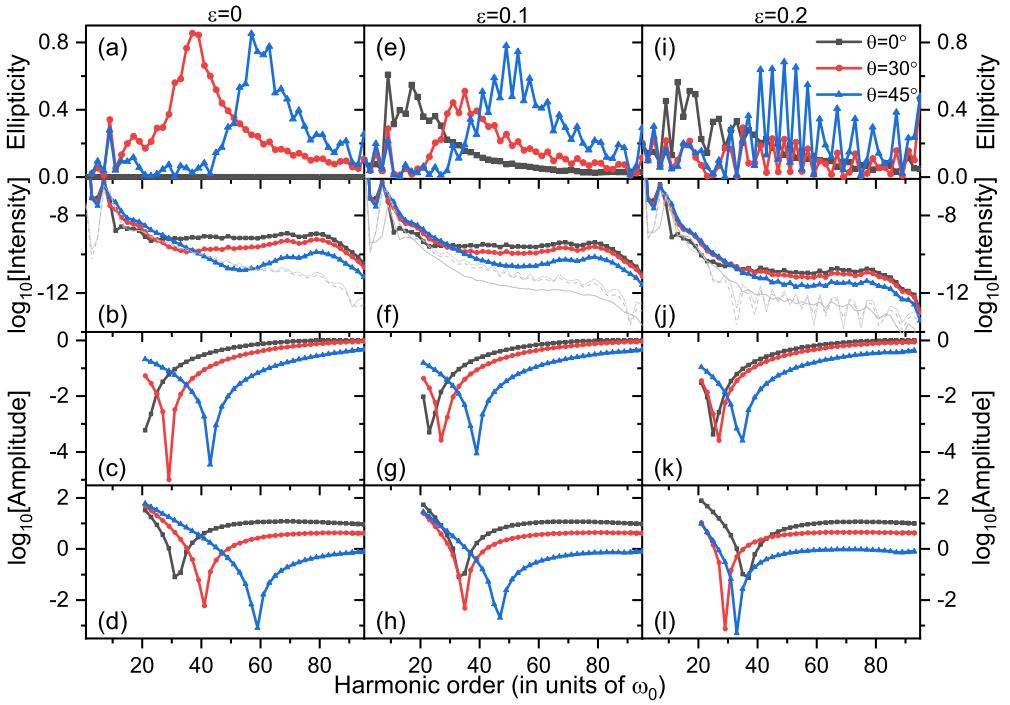

FIG. 3. Ellipticity (the first row), spectra of parallel harmonics (second), the corresponding function curves $M_s^r(\omega,\theta)$ of Eq. (10) (third), and the corresponding recombination dipoles $\mathbf{e}_\parallel \cdot \mathbf{d}_r(\mathbf{p})$ calculated with the Coulomb continuum wave (fourth) for aligned molecules H_2^+ at different angles of $\theta = 0^\circ$ (black square), $\theta = 30^\circ$ (red circle), and $\theta = 45^\circ$ (blue triangle) and different laser ellipticity of $\varepsilon = 0$ (the first column), $\varepsilon = 0.1$ (second), and $\varepsilon = 0.2$ (third). In the second row, spectra of perpendicular harmonics at $\theta = 0^\circ$ (solid), $\theta = 30^\circ$ (dashed), and $\theta = 45^\circ$ (dotted) are also plotted with gray curves for comparison.

These spectral minima are associated with two-center interference and are well described by the corresponding minima in the function curves of Eq. (10) in Fig. 3(c). For simplicity, we will call the function curve of Eq. (10) the dipole from hereon. A careful comparison tells us that the spectrum at $\theta = 0^\circ$ in Fig. 3(b) also shows a minimum at about H21, which is near the threshold, in agreement with the prediction of $M_s^r(\omega,\theta)$ in Fig. 3(c). However, the harmonics at this angle do not show the ellipticity due to the absence of perpendicular harmonics. For the case of a small laser ellipticity of $\varepsilon = 0.1$ in Fig. 3(e), a striking ellipticity plateau of harmonics located around the threshold is observed for $\theta = 0^\circ$, which has been indicated in Fig. 1. For this laser ellipticity in Fig. 3(e), the harmonics at $\theta = 30^\circ$ and 45° also show a remarkable ellipticity peak, the magnitudes of which are somewhat smaller than the corresponding ones in Fig. 3(a). When comparing with the spectra in Fig. 3(f), one can also observe that the large ellipticity of harmonics generally appears at the harmonic orders at which the harmonic spectrum shows a striking minimum, as discussed in the first column of Fig. 3. The positions of the spectral minima in Fig. 3(f) also basically agree with the positions of the dipole minima, as shown in Fig. 3(g). In comparison with the results in Fig. 3(c), one can also observe from Fig. 3(g) that the minima in dipoles for intermediate angles of $\theta = 30^\circ$ and 45° shift somewhat toward lower energy, while the minimum in the dipole of $\theta = 0^\circ$ shifts somewhat toward higher energy. This is due to the influence of the minor component of the elliptical laser field, which changes the recollision angle of HHG. We will address this question in detail in Fig. 4.

Comparing the spectra at different angles in Fig. 3(f), it is clear that the spectrum of $\theta = 0^\circ$ is somewhat lower than those of $\theta = 30^\circ$ and 45° at lower harmonic orders near and

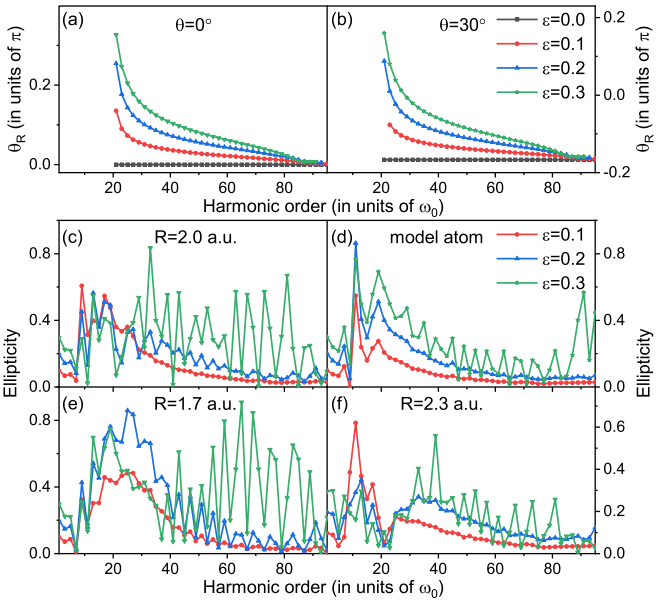

FIG. 4. Recollision angles of HHG short trajectories from aligned molecules H_2^+ at $\theta = 0^\circ$ (a) and $\theta = 30^\circ$ (b) for different laser ellipticity ε. In (c)–(f) we show the ellipticity of harmonics for H_2^+ with $R = 2$ a.u. (c), $R = 1.7$ a.u. (e), and $R = 2.3$ a.u. (f) at $\theta = 0^\circ$ and for a model atom with similar I_p to H_2^+ (d). The laser ellipticity used for obtaining the curves is as shown.

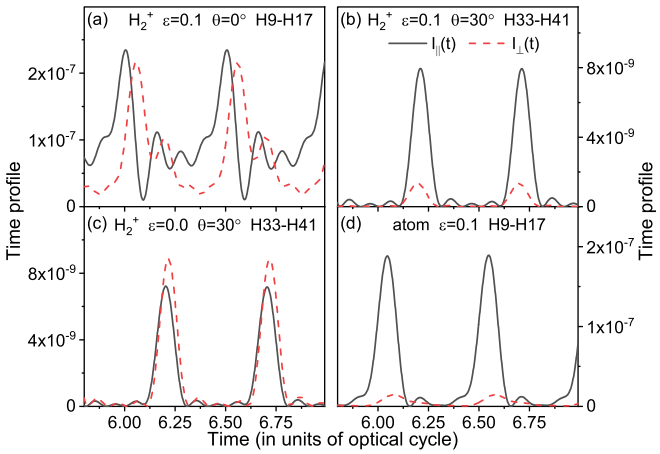

FIG. 5. Trains of pluses $I_{\parallel}(t)$ and $I_{\perp}(t)$ obtained from a specific HHG spectral region for an aligned molecule H_2^+ at $\theta = 0^\circ$ (a) and $\theta = 30^\circ$ (b,c) and for a model atom with similar I_p to H_2^+ (d). In each panel, the laser ellipticity used for obtaining the HHG spectrum and the corresponding specific spectral region are as shown.

below the threshold, but it is remarkably higher than those in the HHG plateau region. Since the yields of below-threshold harmonics for $\theta = 0^\circ$ are one order or several orders of magnitude higher than those in the plateau region for intermediate angles of $\theta = 30^\circ$ and 45°, one can expect that EUV pulses with high ellipticity obtained with the ellipticity hump of $\theta = 0^\circ$ at lower harmonic orders will also be remarkably brighter than those obtained with the plateau harmonics of intermediate angles. We will discuss this point in Fig. 5.

Upon further increasing the laser ellipticity to $\varepsilon = 0.2$, the results in the third column of Fig. 3 are somewhat similar to those in the second column, but the ellipticity of harmonics in Fig. 3(i) is somewhat more irregular than that in Fig. 3(e), and the intensities of spectra in Fig. 3(j) are one order of magnitude lower than those in Fig. 3(f). The remarkable shift of the dipole minima with the change of the laser ellipticity can also be seen in Fig. 3(i). We mentioned that in Figs. 3(j) and 3(k), the agreement between the spectra and the dipoles for the minima is not as remarkable as in other columns of Fig. 3, suggesting that the form of the effective momentum $\mathbf{p}'_{sr}$ used here is more applicable for small ellipticity. In addition, the spectral minima can be influenced by the contributions of excited states to HHG, which are not included in the SFA. By comparison, the intersections of the spectra at different angles match better with those of the relevant dipoles in Fig. 3. Similar phenomena have been discussed in [37,40].

From the results in Fig. 3, one can conclude that for intermediate angles, the large ellipticity of harmonics is also closely associated with the effect of intramolecular interference, which plays an important role in the emission of parallel harmonics and has a relatively small role in the perpendicular harmonics, resulting in a phase difference between parallel and perpendicular harmonics. From the perpendicular spectra of gray curves in the second row of Fig. 3 (see also Fig. 2), one can observe that the perpendicular spectra do not show the striking hollow structure relating to two-center interference, as seen in the corresponding parallel spectra there. On the whole, the intensities of perpendicular spectra gradually decrease with the increase of harmonic order. The influence of two-center interference on the ellipticity of HHG from aligned molecules for intermediate angles in a linearly polarized laser field has been discussed in [14,18–20]. Here, we focus on the case of parallel alignment and elliptically polarized laser fields.

For the case of parallel alignment of $\theta = 0^\circ$, the situation is more complex. As seen in the second column of Fig. 3, although the dipole of $\theta = 0^\circ$ shows a striking minimum near the threshold in Fig. 3(g), the two-center interference minimum is poorly pronounced for the spectral result of $\theta = 0^\circ$ in Fig. 3(f). This is consistent with previous studies that showed that the visibility of two-center interference in the molecular HHG spectra tends to zero as the interference minimum approaches the threshold energy [46]. Accordingly, the contribution of the interference mechanism to the ellipticity of harmonics should also decrease to zero. This prevents the recognition of the interference mechanism as the main cause of ellipticity in the case of the angle θ close to zero. However, the behavior of harmonic ellipticity is very similar here to the atomic case, as shown in Fig. 6 in [25] [see also Fig. 4(d) below], demonstrating the peak near the threshold harmonic. It can therefore be concluded that in this case, the main physics behind the harmonic ellipticity is completely different from that in the case of large angles θ. It is very likely to be the same as in atoms, where the origin of harmonic ellipticity is related mostly to the quantum-mechanical uncertainty of the electron wave-packet motion, as revealed in [17].

On the other hand, the maximum ellipticity in this case falls in the region near or below the threshold, where the intensity of harmonics is much higher than on the plateau. The generation of the strong near- or below-threshold harmonics is not dominated by the recollision mechanism caused by free-bound transitions, but by other mechanisms in which bound-bound transitions are involved. In this case, one can expect that two-center interference effects, which are inherent only in free-bound transitions, play a small role. However, the multiple-center characteristic that differentiates the molecule from the atom may also play a nontrivial role here. We will return to this point later.

It should be stressed that the plane-wave approximation neglects the Coulomb effect on the continuum electron. The use of the effective momentum $\mathbf{p}_k$ instead of $\mathbf{p}$ in the plane wave partly considers the Coulomb effect, but it is not enough for an accurate description [47]. The continuum electron can be better described with the Coulomb continuum wave, as shown in [48,49]. We have also performed simulations calculating the recombination dipole $\mathbf{e}_{\parallel} \cdot \mathbf{d}_r(\mathbf{p}_{sr})$ with the Coulomb wave [50]. Relevant results are shown in the fourth row of Fig. 3. It can be seen that the use of the Coulomb wave improves the comparison between the dipole and the HHG spectrum, especially for higher harmonic orders.

Next, we further discuss the mechanism of the angle-dependent HHG ellipticity observed in Fig. 3, along with analyzing the interference term $M_s^r(\omega, \theta)$ of Eq. (10) in the recombination dipole. In Figs. 4(a) and 4(b), we show the recollision angles θ_R, associated with short electron trajectories and defined in Eq. (10), for $\theta = 0^\circ$ and 30° at different ε. For the case of parallel alignment in Fig. 4(a), on the whole, the recollision angle gradually decreases upon increasing the

harmonic order for a certain laser ellipticity, and it increases with the increase of laser ellipticity for a certain harmonic order. In particular, for $\varepsilon = 0$, the recollision angle is zero and it agrees with the alignment angle of $\theta = 0^\circ$. For the intermediate angle of $\theta = 30^\circ$, the situation is different, as shown in Fig. 4(b). In that case, the absolute value of the recollision angle basically decreases as the laser ellipticity increases, and this decrease is more striking for lower harmonic orders. According to Eq. (10), in the region of $|\theta_R| \in [0, \pi/2]$, as the absolute value of the angle θ_R increases, the value of $\cos\theta_R$ decreases, and the minimal value of the function $M_s^r(\omega, \theta)$ will appear at larger p_{sr}. Therefore, for $\theta = 0^\circ$, the increase of the laser ellipticity, which gives rise to the increase of θ_R, will induce a shift of the minimum of Eq. (10) toward somewhat larger harmonic energy. This situation is reversed for $\theta = 30^\circ$. These analyses explain the results in the third row of Fig. 3, and they shed light on the spectral and polarization results in other rows of Fig. 3.

In comparison with intermediate angles, the maximum ellipticity for $\theta = 0^\circ$ of H_2^+ will appear at lower harmonic energy at which the harmonic spectra usually have larger amplitudes. This effect also holds for other internuclear distances of H_2^+ and for other molecular targets such as N_2 with other symmetries. We will discuss the case of N_2 later. Therefore, the parallel alignment of molecules is preferred for obtaining a bright EUV pulse with high ellipticity. As a comparison, in Figs. 4(c)–4(f), we show the HHG polarization results of H_2^+ at different internuclear distances and laser ellipticity, and we also show the results of the model atom. One can observe that the remarkable polarization phenomenon at lower harmonic energy appears in all of the cases. However, when the results of molecules show an ellipticity hump around the threshold on the whole, the ellipticity curves of the model atom are somewhat sharper. This ellipticity hump for molecules with small R at $\theta = 0^\circ$ observed here is somewhat similar to that for molecules with large R at intermediate angles in a linearly polarized laser field [20]. In [20], it was shown that excited-state effects related to the molecular property play an important role in the ellipticity hump there. In addition, excited-state effects are also important for high ellipticity of lower-order harmonics of molecules with a small R at intermediate angels in a linearly polarized laser field [19]. One can therefore expect that this hump observed here is also closely associated with the multiple-center characteristic of the molecule. Quantum effects relating to this characteristic increase the range of harmonics with large ellipticity, along with forming the ellipticity hump. From the perspective of shaping a short EUV pulse with a broad energy region of harmonics, the ellipticity hump is also preferred, as shown in Fig. 5.

In Fig. 5, we plot trains of pulses $I_\parallel(t)$ and $I_\perp(t)$, obtained from the HHG spectra of H_2^+ at $\theta = 0^\circ$. We also compare the results to cases of H_2^+ at $\theta = 30^\circ$ and to the model atom. The expressions of $I_\parallel(t)$ and $I_\perp(t)$ are as follows [51,52]:

$$I_{\parallel(\perp)}(t) = \left| \int_{\omega_d}^{\omega_u} F_{\parallel(\perp)}(\omega) e^{-i\omega t} d\omega \right|^2. \tag{11}$$

Here, $F_{\parallel(\perp)}(\omega)$ are the parallel and perpendicular HHG spectra of Eq. (1). For H_2^+ at $\theta = 0^\circ$ and for the model atom, we consider the case of $\varepsilon = 0.1$, and our calculations are performed for the spectral region from H9 to H17 (i.e., $\omega_d = 9\omega_0$ and $\omega_u = 17\omega_0$), at which the harmonics have large ellipticity and high intensities. For H_2^+ at $\theta = 30^\circ$, the cases of $\varepsilon = 0$ and 0.1 are considered, and the spectral region integrated is from H33 to H41.

First, for H_2^+ at $\theta = 0^\circ$ with $\varepsilon = 0.1$, the obtained parallel and perpendicular pulses are comparable for intensities with a remarkable time delay, as seen in Fig. 5(a). For the case of $\theta = 30^\circ$ with $\varepsilon = 0.1$ in Fig. 5(b), the pulses of parallel and perpendicular components show a small time delay, and the intensities of perpendicular components are remarkably lower than the parallel ones. By comparison, for $\varepsilon = 0$ in Fig. 5(c), the synthesized parallel and perpendicular pulses show comparable intensities and a small time delay. Note, for $\varepsilon = 0$, the HHG from H_2^+ at $\theta = 0^\circ$ does not show the elliptical-polarization effect due to the absence of perpendicular harmonics. However, the intensities of the pulses shown in Figs. 5(b) and 5(c) for $\theta = 30^\circ$ are one order of magnitude lower than those in Fig. 5(b) for $\theta = 0^\circ$. The results of the model atom in Fig. 5(d) are somewhat similar to those in Fig. 5(b), with the perpendicular pulse showing small intensities. The results in Fig. 5 support our previous discussions that the harmonics of molecules with parallel alignment are preferred for obtaining a bright elliptically polarized EUV pulse.

To confirm our discussions above, we have also performed calculations for the N_2 molecule with a $3\sigma_g$ valence orbital, which can be operated more easily in experiments. To simulate the HHG of N_2 with $I_p = 0.57$ a.u., we have used the model potential $V(\mathbf{r})$ [53] with the form $V(\mathbf{r}) = -[(Z - Z_0)e^{-\rho\mathbf{r}_1^2} + Z_0]/\sqrt{\zeta + \mathbf{r}_1^2} - [(Z - Z_0)e^{-\rho\mathbf{r}_2^2} + Z_0]/\sqrt{\zeta + \mathbf{r}_2^2}$. The expressions of $\mathbf{r}_{1(2)}^2$ are as for H_2^+. The relevant parameters used are $Z = 5$, $Z_0 = 0.5$, $R = 2.079$ a.u., $\zeta = 0.5$, and $\rho = 1.555$. Because of the smaller ionization potential for N_2 compared with H_2^+, here we use a weaker driving laser intensity of $I = 1.2 \times 10^{14}$ W/cm^2 and a longer laser wavelength of $\lambda = 1400$ nm. Relevant results at different angles θ with $\varepsilon = 0.1$ are presented in Fig. 6. For comparison, the results of a model atom with similar I_p to N_2 are also presented here. We focus on lower harmonic orders near the threshold. One can observe from Fig. 6(a) that the parallel spectra of N_2 at $\theta = 0^\circ$ show larger intensities than those in the cases of other angles and the model atom. Around H25, somewhat higher than the threshold harmonic of H19, the harmonics of $\theta = 0^\circ$ also show an ellipticity hump, more remarkable than in other cases, as seen in Fig. 6(b). We mention that in our extended simulations in which the laser parameters are changed, this hump holds. The trains of pulses obtained from the spectral region of H23–H31 for N_2 at the parallel alignment and for the model atom are presented in Figs. 6(c) and 6(d). When the results of the model atom for parallel and perpendicular pulses of $I_\parallel(t)$ and $I_\perp(t)$ do not show an obvious time delay in Fig. 6(d), the time delay for the results of N_2 can be clearly identified in Fig. 6(c). In addition, the relative intensity of the perpendicular pulse in comparison with the parallel one is also remarkably larger for N_2 than for the model atom. The results also support the

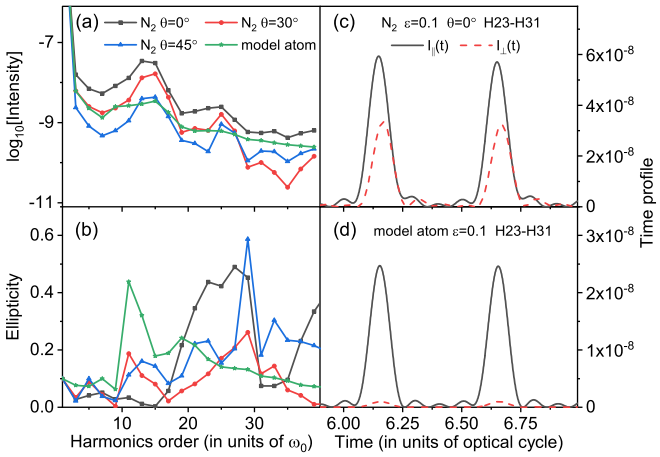

FIG. 6. Spectra of parallel harmonics (a) and ellipticity of harmonics (b) for aligned molecules N_2 at $\theta = 0^\circ$ (black square), $\theta = 30^\circ$ (red circle), $\theta = 45^\circ$ (blue triangle), and for a model atom with similar I_p to N_2 (green star), obtained with short-trajectory TDSE simulations. In (c) and (d), we show trains of pulses $I_\parallel$ (black solid) and $I_\perp$ (red dashed) obtained from a specific HHG spectral region of H23–H31 for N_2 (c) and the model atom (d). The laser parameters used are $I = 1.2 \times 10^{14}$ W/cm^2 and $\lambda = 1400$ nm with $\varepsilon = 0.1$.

above discussion that the parallel alignment is preferred for generating a strong elliptically polarized EUV pulse.

We mention that in [12] for experimental studies of the N_2 molecule with a linearly polarized laser field, it is shown that the ellipticity of harmonics is zero at $\theta = 0^\circ$ and 90° and is maximized at intermediate angles around $\theta = 50^\circ$. Our extended simulations with similar laser parameters to those previous experiments ($I = 2 \times 10^{14}$ W/cm^2, $\lambda = 800$ nm, and $\varepsilon = 0$) reproduce the experimental results, with the ellipticity of the H17–H27 harmonics peaking around $\theta = 50^\circ$. When increasing the laser ellipticity with other laser parameters unchanged in our extended simulations, the ellipticity of harmonics at $\theta = 0^\circ$ begins to increase remarkably, and for $\varepsilon = 0.1$, the results obtained for 800 nm are similar to those shown in Fig. 6. However, in our calculations for N_2, we use the model potential and single-electron approximation. For real N_2 in experiments, multiple-electron effects can also play an important role in the HHG ellipticity. In addition, in our simulations we assume that the molecule is perfectly aligned, while in real experiments perfect alignment is impossible. Therefore, the theoretical predictions made here need to be checked further in comparison with experimental studies.

IV. SUMMARY

In conclusion, we have studied the polarization properties of HHG from aligned molecules in strong elliptically polarized laser fields with small laser ellipticity. We have shown that the addition of the vertical component of the laser field with a small intensity has important influences on not only the yields but also the polarization of harmonics. In particular, for the parallel alignment of the molecule, for which the perpendicular harmonics disappear in a linearly polarized laser field, the addition of the small vertical component induces a strong emission of perpendicular harmonics and an accompanying high ellipticity of harmonics near or below the threshold with the formation of an ellipticity hump. We show that the phenomenon is related mostly to the quantum-mechanical uncertainty of the electron wave-packet motion, and it holds for molecules with different internuclear distances and symmetries. By comparison, the HHG ellipticity for larger alignment angles appears at higher harmonic orders located in the plateau region of the HHG spectra, and it can be attributed to the effects of two-center interference. Because the harmonics near or below the threshold usually have remarkably higher intensities than those in the HHG plateau, the ellipticity hump for the parallel alignment suggests a manner for generating bright elliptically polarized EUV pulses.

ACKNOWLEDGMENTS

This work was supported by the National Key Research and Development Program of China (Grant No. 2018YFB0504400), and the National Natural Science Foundation of China (Grants No. 11904072 and No. 91750111).

[1] A. McPherson, G. Gibson, H. Jara, U. Johann, T. S. Luk, I. A. McIntyre, K. Boyer, and C. K. Rhodes, Studies of multiphoton production of vacuum-ultraviolet radiation in the rare gases, J. Opt. Soc. Am. B **4**, 595 (1987).

[2] A. L'Huillier, K. J. Schafer, and K. C. Kulander, Theoretical aspects of intense field harmonic generation, J. Phys. B **24**, 3315 (1991).

[3] X.-M. Tong and S.-I. Chu, Theoretical study of multiple high-order harmonic generation by intense ultrashort pulsed laser fields: A new generalized pseudospectral time-dependent method, Chem. Phys. **217**, 119 (1997).

[4] M. Lein, N. Hay, R. Velotta, J. P. Marangos, and P. L. Knignt, Role of the Intramolecular Phase in High-Order Harmonic Generation, Phys. Rev. Lett. **88**, 183903 (2002).

[5] J. Itatani, J. Levesque, D. Zeidler, H. Niikura, H. Pépin, J. C. Kieffer, P. B. Corkum, and D. M. Villeneuve, Tomographic imaging of molecular orbitals, Nature (London) **432**, 867 (2004).

[6] P. B. Corkum and F. Krausz, Attosecond science, Nat. Phys. **3**, 381 (2007).

[7] G. Vampa, C. R. McDonald, G. Orlando, D. D. Klug, P. B. Corkum, and T. Brabec, Theoretical Analysis of High-Harmonic Generation in Solids, Phys. Rev. Lett. **113**, 073901 (2014).

[8] Z. Tao, C. Chen, T. Szilvasi, M. Keller, M. Mavrikakis, H. Kapteyn, and M. Murnane, Direct time-domain observation of attosecond final-state lifetimes in photoemission from solids, Science **353**, 62 (2016).

[9] N. T. Dejean and A. Rubio, Atomic-like high-harmonic generation from two-dimensional materials, Sci. Adv. **4**, eaao5207 (2018).

[10] P. B. Corkum, Plasma Perspective on Strong Field Multiphoton Ionization, Phys. Rev. Lett. **71**, 1994 (1993).

[11] M. Lewenstein, Ph. Balcou, M. Yu. Ivanov, A. L'Huillier, and P. B. Corkum, Theory of high-harmonic generation by low-frequency laser fields, Phys. Rev. A **49**, 2117 (1994).

[12] X. Zhou, R. Lock, N. Wagner, W. Li, H. C. Kapteyn, and M. M. Murnane, Elliptically Polarized High-Order Harmonic Emission from Molecules in Linearly Polarized Laser Fields, Phys. Rev. Lett. **102**, 073902 (2009).

[13] J. Levesque, Y. Mairesse, N. Dudovich, H. Pépin, J.-C. Kieffer, P. B. Corkum, and D. M. Villeneuve, Polarization State of High-Order Harmonic Emission from Aligned Molecules, Phys. Rev. Lett. **99**, 243001 (2007).

[14] S.-K. Son, D. A. Telnov, and S.-I. Chu, Probing the origin of elliptical high-order harmonic generation from aligned molecules in linearly polarized laser field, Phys. Rev. A **82**, 043829 (2010).

[15] S. Ramakrishna, P. A. J. Sherratt, A. D. Dutoi, and T. Seideman, Origin and implication of ellipticity in high-order harmonic generation from aligned molecules, Phys. Rev. A **81**, 021802(R) (2010).

[16] P. A. J. Sherratt, S. Ramakrishna, and T. Seideman, Signatures of the molecular potential in the ellipticity of high-order harmonics from aligned molecules, Phys. Rev. A **83**, 053425 (2011).

[17] V. V. Strelkov, A. A. Gonoskov, I. A. Gonoskov, and M. Yu. Ryabikin, Origin for Ellipticity of High-Order Harmonics Generated in Atomic Gases and the Sublaser-Cycle Evolution of Harmonic Polarization, Phys. Rev. Lett. **107**, 043902 (2011).

[18] S. J. Yu, B. Zhang, Y. P. Li, S. P. Yang, and Y. J. Chen, Ellipticity of odd-even harmonics from oriented asymmetric molecules in strong linearly polarized laser fields, Phys. Rev. A **90**, 053844 (2014).

[19] F. L. Dong, Y. Q. Tian, S. J. Yu, S. Wang, S. P. Yang, and Y. J. Chen, Polarization properties of below-threshold harmonics from aligned molecules H_2^+ in linearly polarized laser fields, Opt. Express **23**, 18106 (2015).

[20] W. Y. Li, F. L. Dong, S. J. Yu, S. Wang, S. P. Yang, and Y. J. Chen, Ellipticity of near-threshold harmonics from stretched molecules, Opt. Express **23**, 31010 (2015).

[21] K. S. Budil, P. Salières, A. L'Huillier, T. Ditmire, and M. D. Perry, Influence of ellipticity on harmonic generation, Phys. Rev. A **48**, R3437 (1993).

[22] P. Dietrich, N. H. Burnett, M. Ivanov, and P. B. Corkum, High-harmonic generation and correlated two-electron multiphoton ionization with elliptically polarized light, Phys. Rev. A **50**, R3585 (1994).

[23] P. Antoine, B. Carré, A. L'Huillier, and M. Lewenstein, Polarization of high-order harmonics, Phys. Rev. A **55**, 1314 (1997).

[24] V. V. Strelkov, Theory of high-order harmonic generation and attosecond pulse emission by a low-frequency elliptically polarized laser field, Phys. Rev. A **74**, 013405 (2006).

[25] V. V. Strelkov, M. A. Khokhlova, A. A. Gonoskov, I. A. Gonoskov, and M. Yu. Ryabikin, High-order harmonic generation by atoms in an elliptically polarized laser field: Harmonic polarization properties and laser threshold ellipticity, Phys. Rev. A **86**, 013404 (2012).

[26] M. V. Frolov, N. L. Manakov, T. S. Sarantseva, and A. F. Starace, High-order-harmonic-generation spectroscopy with an elliptically polarized laser field, Phys. Rev. A **86**, 063406 (2012).

[27] T. S. Sarantseva, A. A. Silaev, and N. L. Manakov, High-order-harmonic generation in an elliptically polarized laser field: analytic form of the electron wave packet, J. Phys. B **50**, 074002 (2017).

[28] R. Velotta, N. Hay, M. B. Mason, M. Castillejo, and J. P. Marangos, High-Order Harmonic Generation in Aligned Molecules, Phys. Rev. Lett. **87**, 183901 (2001).

[29] I. V. Litvinyuk, K. F. Lee, P. W. Dooley, D. M. Rayner, D. M. Villeneuve, and P. B. Corkum, Alignment-Dependent Strong Field Ionization of Molecules, Phys. Rev. Lett. **90**, 233003 (2003).

[30] T. Kanai, S. Minemoto, and H. Sakai, Ellipticity Dependence of High-Order Harmonic Generation from Aligned Molecules, Phys. Rev. Lett. **98**, 053002 (2007).

[31] Y. Mairesse, N. Dudovich, J. Levesque, M. Yu. Ivanov, P. B. Corkum, and D. M. Villeneuve, Electron wavepacket control with elliptically polarized laser light in high harmonic generation from aligned molecules, New. J. Phys. **10**, 025015 (2008).

[32] S. Odžak and D. B. Milošević, Role of ellipticity in high-order harmonic generation by homonuclear diatomic molecules, Phys. Rev. A **82**, 023412 (2010).

[33] H. Yang, P. Liu, R. X. Li, and Z. Z. Xu, Ellipticity dependence of the near-threshold harmonics of H_2 in an elliptical strong laser field, Opt. Express **21**, 028676 (2013).

[34] Y. Q. Xia and A. Jaroń-Becker, Multielectron contributions in elliptically polarized high-order harmonic emission from nitrogen molecules, Opt. Lett. **39**, 1461 (2014).

[35] M. D. Feit, J. A. Fleck, Jr., and A. Steiger, Solution of the Schrödinger equation by a spectral method, J. Comput. Phys. **47**, 412 (1982).

[36] N. L. Phan, C. T. Le, V. H. Hoang, and V. H. Le, Odd-even harmonic generation from oriented CO molecules in linearly polarized laser fields and the influence of the dynamic core-electron polarization, Phys. Chem. Chem. Phys. **21**, 24177 (2019).

[37] Y. J. Chen, J. Liu, and B. Hu, Reading molecular messages from high-order harmonic spectra at different orientation angles, J. Chem. Phys. **130**, 044311 (2009).

[38] P. Salières, B. Carré, L. Le Déroff, F. Grasbon, G. G. Paulus, H. Walther, R. Kopold, W. Becker, D. B. Milošević, A. Sanpera, and M. Lewenstein, Feynman's path-integral approach for intense-laser-atom interactions, Science **292**, 902 (2001).

[39] M. Lewenstein, P. Salières, and A. L'Huillier, Phase of the atomic polarization in high-order harmonic generation, Phys. Rev. A **52**, 4747 (1995).

[40] Y. J. Chen and B. Hu, Role of ionization in orientation dependence of molecular high-order harmonic generation, J. Chem. Phys. **131**, 244109 (2009).

[41] X. J. Xie, S. J. Yu, W. Y. Li, S. Wang, and Y. J. Chen, Routes of odd-even harmonic emission from oriented polar molecules, Opt. Express **26**, 18578 (2018).

[42] Y. J. Chen and B. Hu, Intense field ionization of diatomic molecules: Two-center interference and tunneling, Phys. Rev. A **81**, 013411 (2010).

[43] W. Y. Li, S. Wang, Y. Z. Shi, S. P. Yang, and Y. J. Chen, Probing the structure of stretched molecular ions with high-harmonic spectroscopy, J. Phys. B **50**, 085003 (2017).

[44] C. Chen, D. X. Ren, X. Han, S. P. Yang, and Y. J. Chen, Time-resolved harmonic emission from aligned molecules in orthogonal two-color fields, Phys. Rev. A **98**, 063425 (2018).

[45] X.-M. Tong and S.-I. Chu, Probing the spectral and temporal structures of high-order harmonic generation in intense laser pulses, Phys. Rev. A **61**, 021802(R) (2000).

[46] I. A. Gonoskov and M. Yu. Ryabikin, Two-center interference in high harmonic generation from diatomic molecule: detailed numerical study, J. Mod. Opt. **55**, 2685 (2008).

[47] Y. P. Li, S. J. Yu, X. Y. Duan, Y. Z. Shi, and Y. J. Chen, Wavelength dependence of high-harmonic yield from aligned molecules: roles of structure and electron dynamics, J. Phys. B **49**, 075603 (2016).

[48] M. F. Ciappină, C. C. Chirila, and M. Lein, Influence of Coulomb continuum wave functions in the description of high-order harmonic generation with H_2^+, Phys. Rev. A **75**, 043405 (2007).

[49] A.-T. Le, R. D. Picca, P. D. Fainstein, D. A. Telnov, M. Lein, and C. D. Lin, Theory of high-order harmonic generation from molecules by intense laser pulses, J. Phys. B **41**, 081002 (2008).

[50] Y. J. Chen, L. B. Fu, and J. Liu, Asymmetric Molecular Imaging through Decoding Odd-Even High-Order Harmonics, Phys. Rev. Lett. **111**, 073902 (2013).

[51] P. Antoine, A. L. Huillier, and M. Lewenstein, Attosecond Pulse Trains using High-Order Harmonics, Phys. Rev. Lett. **77**, 1234 (1996).

[52] Y. Z. Shi, S. Wang, F. L. Dong, Y. P. Li, and Y. J. Chen, Classical effect for enhanced high harmonic yield in ultrashort laser pulses with a moderate laser intensity, J. Phys. B **50**, 065004 (2017).

[53] S. Wang, J. Cai, and Y. J. Chen, Ionization dynamics of polar molecules in strong elliptical laser fields, Phys. Rev. A **96**, 043413 (2017).